Thermal Modeling of Large Electrolytic Capacitors Using FEM and Considering the Internal Geometry

Lledo-Ponsati, Tomas; Bahman, Amir Sajjad; Iannuzzo, Francesco; Montesinos-Miracle, Daniel; Galceran-Arellano, Samuel

Published in:
IEEE Journal of Emerging and Selected Topics in Power Electronics

DOI (link to publication from Publisher):
10.1109/JESTPE.2021.3089899

Publication date:
2021

Document Version
Accepted author manuscript, peer reviewed version

JESTPE-2020-07-0759.R4

Thermal Modeling of Large Electrolytic Capacitors Using FEM and Considering the Internal Geometry

Tomàs Lledó-Ponsati[1], *Student Member, IEEE*, Amir Sajjad Bahman[2], *Senior Member, IEEE*, Francesco Iannuzzo[2], *Senior Member, IEEE*, Daniel Montesinos-Miracle[1], *Senior Member, IEEE*, Samuel Galceran-Arellano[1]

Abstract—This paper focuses on developing a finite element method (FEM) model for large capacitors thermal modeling and reliability analysis. Thermal modeling for capacitors is critical since the capacitor's lifetime depends on the capacitor's maximum temperature. Typically, capacitors have been modeled as a solid element, not considering the capacitor's internal geometry, leading to temperature estimation errors and requiring extensive testing to adjust the model. The presented methodology to develop the model considers the internal geometry to obtain a reliable model, with sufficient simplicity to adapt the methodology to any electrolytic capacitor. To achieve good results, the capacitor's winding is modeled as an anisotropic material to reproduce appropriately the behavior of the layers of aluminum and paper soaked in electrolyte. The results of the simulations match the experimental results closely, therefore validating the utility of the model.

Index terms—Finite element methods, capacitors, reliability, thermal model.

I. Introduction

The thermal analysis of capacitors is critical when analyzing their reliability since the estimated lifetime is determined mainly by the temperature of the capacitor's hottest point [1]. Commonly, for large electrolytic capacitors is assumed that the lifetime of a capacitor (L) is reduced a half for every ten-degree increment in the operating temperature (T) [1], [2], as showed in equations (1) and (2). L_0 is the rated lifetime at the rated operating temperature (T_0) and the rated voltage (V_0). As can be expected, the operating voltage (V) also plays a role in reliability.

$$L = L_0 \cdot \left(\frac{V}{V_0}\right)^{-n} \cdot 2^{\frac{T_0 - T}{10}} \quad (1)$$

$$n = 5 \; for \; 0.8 \leq \frac{V}{V_0} \leq 1 \quad (2)$$

Therefore, it is evident that thermal modeling is of capital importance when analyzing its reliability.

Typically, electrolytic capacitors fail in three modes [1]. The first one is open circuit mode due to vibrations that can cause a disconnection of the terminals or due to a self-healing dielectric breakdown.

The second one is a short circuit mode. It is caused by a dielectric breakdown of the oxide layer. Mainly due to overvoltage or defects in the dielectric layer caused during the manufacture [3].

The last failure mode is a wear-out phenomenon and is the most common [4]. The failure mechanisms that can lead to a wear-out of the capacitor are diverse. Typically, electrolyte evaporation has been considered the primary mechanism. The electrolyte evaporation leads to an increase in the equivalent series resistance (*ESR*) since it is highly dependent on the electrolyte [5]. Nevertheless, for large electrolytic capacitors, other effects, such as the de-passivation of the cathode foil, play a more prominent role [6]. This mechanism consists of the growth on the cathode foil's surface of an aluminum oxide (Al_2O_3) layer, leading to an increase in the thickness of the capacitor's dielectric material, leading to a reduction of the capacitance [7].

Traditionally, capacitors have been modeled using different approaches [8], [9], [10], and [11]. The number of publications approaching in-depth the modeling of electrolytic capacitors and considering the capacitor's internal structure is low, especially in recent years. Most of the literature available is already more than fifteen years old. For example, [8] and [9] analyze the electrolytic capacitors' thermal modeling by performing a series of thermal tests with the capacitors' internal layers. In [10], the authors explore the improvement in electrolytic capacitors' thermal dissipation, thanks to an extended cathode. In [11], the reduction in the case to ambient thermal resistance is analyzed, thanks to the plastic insulation sleeve at the exterior of the capacitor and other solutions.

Lately, capacitors have been modeled as solid elements when using a finite element method (FEM) model [12]. For large electrolytic capacitors, typically, a solid cylinder is used. This approach has been followed because the capacitor's thermal load is determined mainly by the air's temperature surrounding the capacitor. It is especially relevant in capacitor bank modeling [12]. The thermal properties of this solid object are determined by performing tests with the real equipment. Although useful, this method requires developing a test bench to characterize the capacitors and obtain the thermal properties that are later introduced in the FEM model. It will also require capacitors fitted with a thermocouple, which is not a standard feature for off-the-shelf capacitors.

A different approach is proposed in this paper to overcome the limitations of the previous methods presented. The proposed method models the capacitor, trying to replicate the internal structure as close as possible to reality. This way, the materials' thermal properties can be implemented in the model, and there is no need to characterize them. Enhancing the re-usability of this methodology for different capacitors and reducing the time invested in creating the model.

On the other hand, following this approach requires an in-depth knowledge of the capacitor's internal geometry since it plays a critical role. The thickness of the foils and the isolation papers strongly affect the thermal properties. The geometry can be obtained directly from the capacitor's manufacturer or by realizing dimensional measurements on the capacitor under study. For this paper, the second methodology has been followed.

External and internal measurements are necessary to model the capacitor. The external measurements can be obtained easily with a caliper. The internal measurements

[1] Centre d'Innovació Tecnològica en Convertidors Estàtics i Accionaments (CITCEA-UPC), Departament d'Enginyeria Elèctrica, Universitat Politècnica de Catalunya.
ETS d'Enginyeria Industrial de Barcelona, Av. Diagonal, 647, Pl. 2. 08028 Barcelona, Spain. Tel: +34 934016727, Fax: +34 934017433

[2] Centre of Reliable Power Electronics (CORPE), Aalborg University (AAU)

can be obtained using a non-invasive method such as a CT (computed tomography) scan. Alternatively, tearing apart the capacitor. The necessary measurements include the thickness of the enclosing can and the enclosed capacitor dimensions, which can be measured with a caliper. The thickness of the anode and cathode foils can be measured by stacking a known number of layers and measuring its total thickness. Finally, the number of turns of the capacitor can be obtained by counting the number of layers in a known distance following a radial line.

In the paper is done a complete analysis of the capacitor's internal elements. With this analysis, it is possible to study the necessary simplifications of the capacitor's winding to model it as an anisotropic material. The paper also provides the guidelines to be followed for modeling a capacitor with the proposed methodology and an example with a specific capacitor.

The paper is organized as follows. A review of the different modeling methods available and an analysis of their advantages and disadvantages. An analysis of the internal structure of electrolytic capacitors and a presentation of the simplifications done to model the capacitor. Next, a validation of the previous section's assumptions is done by comparing the simplified approach with a model considering its internal geometry. After the simplifications are validated, a model is developed for a determined capacitor. The results obtained from the simulations are compared with real measurements. Next, the model obtained is compared with the manufacturer's model by performing a mission profile analysis of the capacitor. Finally, the conclusions are presented.

II. Electrolytic Capacitors Modeling Methods

The different methods presented in the literature are analyzed to identify their strengths and weaknesses. Afterward, a new approach is proposed that will help to obtain a better thermal model.

A. *Empirical determination of the thermal properties*

The first approaches to capacitor thermal modeling were made using empirical measurements in the capacitor [8]. The thermal properties of the capacitor winding are determined by performing thermal tests on them. This method requires the development of specific equipment to do the proper measurements and is extremely sensitive to an improper assembly of these specific setups. The author measured the thermal impedance in the axial and the radial directions by performing a series of tests with the stacked layers found inside a capacitor, i.e., the anode and the cathode foils and the paper isolators soaked in electrolyte. As the author explains in his paper, it is crucial to maintain the aluminum foils and the paper isolators compressed together as they will be inside a capacitor. Fig. 1 shows the setup necessary [8] to determine the winding's thermal resistance in the radial direction. It is necessary to stack the multiple layers of a capacitor together, keeping them compressed, as stated previously. The setup requires a controlled power source and several thermocouples to measure the temperature at different points. Finally, everything must be isolated in the sides to allow power dissipation only in the vertical axis.

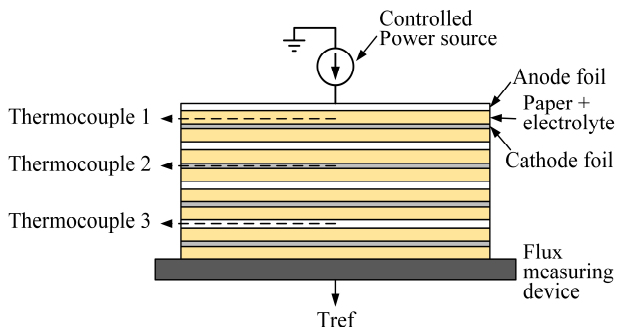

Fig. 1: Setup implemented in [8] to measure the radial conductivity of electrolytic capacitors.

The thermal dissipation from the can to the ambient is modeled as a constant heat convection coefficient and a constant radiation coefficient.

As it is evident, this approach is complicated because it requires the development of specific tools used to model the capacitor.

In addition, the equations obtained are complex and challenging to operate with. Some authors have followed a similar approach but simplifying the heat dissipation to the ambient by using FEM modeling [9].

It has some other drawbacks; the terminals of the capacitor are not taken into account. Therefore, there is no possibility of considering heat dissipation through them. Neither is it possible to consider heat dissipation in the terminals' soldering with the anode and cathode foils. Although, this is more relevant for small electrolytic capacitors rather than for large capacitors.

B. *Thermal network adjustment to empirical measurements*

Most of the electrolytic capacitors' thermal analyses are done by performing controlled tests with a capacitor fitted with one or multiple thermocouples. With the aid of specific equipment, the current ripple is fixed to a known value to fix the desired power losses. An experimental thermal network is obtained directly from the temperature measurements. There are plenty of examples in the recent literature following this approach. Some examples obtain a complete thermal network, including convection and radiation to the ambient, [13], [14], and others obtain only the capacitor's thermal network. A solid element is implemented in a FEM simulation with the appropriate properties to match the behavior, and the case to ambient dissipation is simulated [12], [15]. This helps implement the thermal coupling between different capacitors or changes in the ambient dissipation, Fig. 2.

This method, although proved to be efficient, has one major flaw. To simulate the temperature on the inside of the capacitor, it is necessary to test the capacitor at the nominal current ripple to adjust the thermal properties of the material composing the cylinder under analysis in the FEM model. It also requires a thermocouple for the capacitor to perform the tests, making it unsuitable for off-the-shelf capacitors.

C. *Other approaches*

There are other examples following the same approach presented in this paper. In [16] and [17], the authors present two analyses with the anisotropic winding modeling

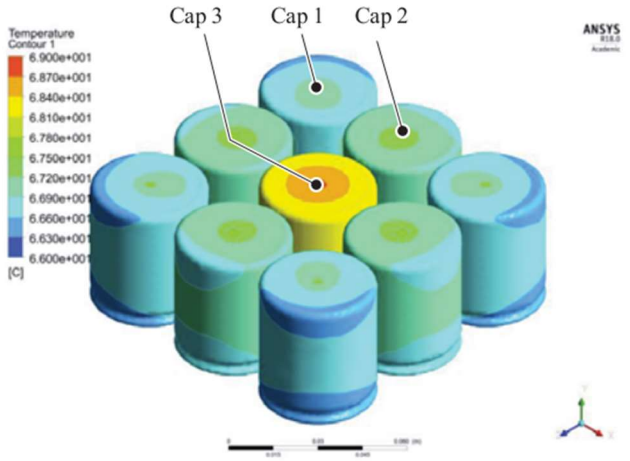

Fig. 2: FEM simulation of a bank of capacitors modelled as solid elements [12].

approach but focused on film capacitors. However, both analyses are limited to steady-state. Additionally, neither [16] nor [17] provide information about modeling the capacitor case and the thermal interface between the winding and the case. This is of paramount importance for electrolytic capacitors because the cathode foil is used to improve the dissipation by connecting it to the case.

In [18] and [19], the authors apply the same approach to electrolytic capacitors. However, they lack a proper analysis considering the internal structure completely [18] or lack information on implementing the model [19]. Both papers consider the winding an anisotropic material and calculate the winding's thermal conductivity as the weighted average considering the different materials' volume.

However, these previous references use the model but do not justify its validity. They lack a proper analysis of a capacitor's interior. None of them provides sufficient evidence that simplifying the winding as an anisotropic material is acceptable from a thermal perspective. Additionally, none of the provided references compares the simulation results with experimental results. Moreover, the procedure followed to obtain the necessary parameters to generate the model is unknown. The presence of the extended cathode is not mentioned in any of the papers. Finally, none of them considers the aluminum oxide layer of the anode foil. This layer cannot be despised due to the high etching of the anode foil. None of the previous works provides evidence that this layer can be eliminated from the analysis without impacting the final results. Its relevance has not been assessed, and it is worth checking.

The current paper provides a thorough analysis of this method. An exhaustive analysis of the capacitor's internal elements is done. Next, the necessary parameters' obtention to develop the model is provided with an understandable explanation and replicable methods. The different simplifications applied to the method are analyzed. The impact of the aluminum oxide layer on the thermal properties of the winding is assessed. The simplification of the winding as an anisotropic material is studied with the help of FEM simulations. A comparative analysis between a simplified model and a model with all the internal layers is done. Finally, the performance of the obtained FEM model is compared with experimental results. This paper includes a transient analysis and presents a complete analysis of the winding and the interface with the case and ambient.

Implementing this method helps to obtain a thermal model for the capacitor and eliminates the need to perform tests with a capacitor fitted with a thermocouple. It also helps to implement this capacitor into a bigger FEM model. Furthermore, the method can be applied to off-the-shelf capacitors.

The proposed method provides a thermal model based only on simulations. This can generate doubts for future users that might add thermal measurements in the capacitor to ensure the model's validity. However, this is an issue that has been faced previously in the field of power electronics. The thermal networks for power modules have been largely analyzed with the help of FEM simulations [20], and the analysis validity has been proved [21], [22]. The models obtained with FEM simulations are trusted, and the same is expected to happen with the proposed method. The more it is used, the more it is trusted by the users.

The proposed method's main advantage is its easiness of implementation as soon as the necessary parameters are known. Therefore, this method might be helpful to capacitor manufacturers, for example. They know all the information necessary. With a reasonable effort, it is possible to develop a FEM model with good performance.

However, the procedure is less straightforward for final users if the capacitor's manufacturer is unwilling to share the relevant data. In this paper, the necessary data is obtained with two different approaches. First, with a non-invasive measurement with the help of a CT scan. And second, with an invasive method, tearing apart the capacitor. The first approach is costly and time-consuming. However, the second method cannot be considered difficult, expensive, or excessively time-consuming. It only requires cutting in half a capacitor and measure the relevant parameters, no more than one day of work. A similar approach is followed to develop FEM models of power modules [23]. As stated previously, it is a standard procedure in the literature.

III. Electrolytic Capacitor Internal Analysis

A. *Capacitor characterization*

The electrolytic capacitor's operation principle is based on the dielectric properties of alumina or aluminum oxide (Al_2O_3). Typically, they are made of three different layers rolled together to obtain a cylindrical shape.

The positive terminal of the capacitor is connected to the anode foil. It consists of an aluminum foil treated with an anodization process to generate a layer of Al_2O_3 in the surface with a controlled thickness that will act as the capacitor's dielectric material. The anodization of the capacitor is done on both sides of the foil.

The electrolytic fluid is placed together with a paper layer between the anode foil and the cathode foil. The electrolytic fluid has good conductive properties to ensure a good connection with the cathode foil.

The last layer is the cathode, connected to the negative terminal of the capacitor. This layer is an aluminum layer that has been superficially treated with a passivation to prevent a growth in the external thin aluminum oxide layer that is grown naturally. Non-polarized capacitors also have an Al_2O_3 layer on the second foil surface, but they are

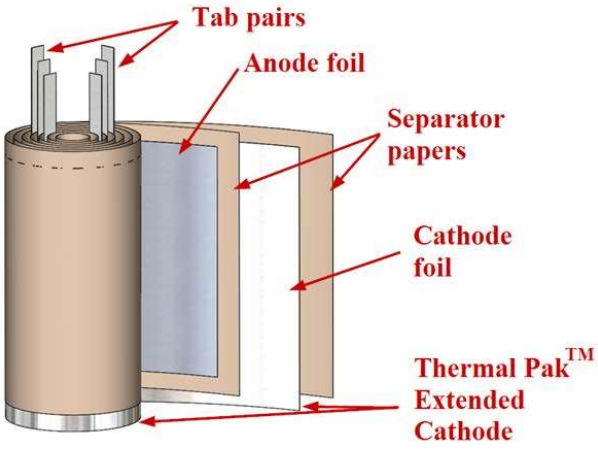

Fig. 3: Structure of the capacitor winding. Source: CDE [4].

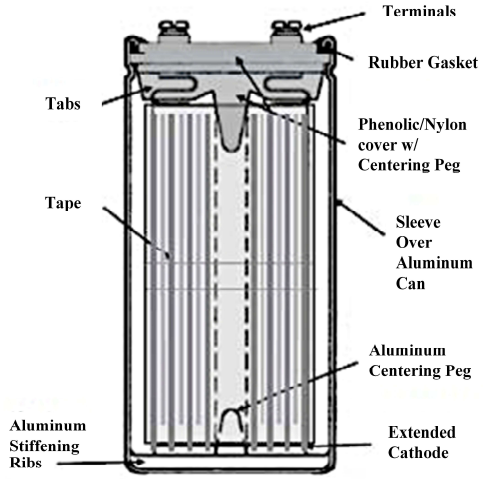

Fig. 4: Capacitor assembly including the extended cathode. Source: CDE [4].

uncommon. To decrease the winding's thermal resistance to the can, usually, the cathode foil is extended, and it makes contact with the base of the can enclosing the capacitor [24]. The paper placed between anode and cathode is also extended in the superior part of the capacitor. The lid applies force into the extended paper to ensure that the extended cathode has good contact with the can's base. Since the cathode foil is thin, the material is crushed, ensuring good thermal contact, Fig. 3 and Fig. 4. Finally, a layer of paper soaked in electrolyte is placed next to the cathode.

For large electrolytic capacitors, each layer's thickness moves in a range between 10—300 µm, and the number of layers with the capacitor winded can go up to more than 50 with a total diameter of more than 50 mm. If it is considered that the total height of the rolled capacitor can exceed 100 mm, it is evident that it is complicated to model a capacitor considering all the layers. The number of elements used in the FEM model will be too high due to the need to use small elements in the foils combined with the high number of elements due to the capacitor's total dimensions.

The solution to this problem is to approach the capacitor winding as an anisotropic material considering polar coordinates, Fig. 5 and Fig. 6. In the radial axis (r), the thermal resistance is the series connection of the paper soaked in electrolyte thermal resistance and the aluminum foils. In the vertical axis (z) and the angular coordinate (φ), the thermal resistance is equivalent to the four layers' parallel connection.

The capacitor EPCOS B43564A6278M000 [25] will be analyzed. The main capacitor characteristics are summarized in Table I

TABLE I: CAPACITOR PARAMETERS AND RELEVANT DIMENSIONS

Parameter	Value
Capacitor maximum voltage (V)	500
Capacitance (µF)	2700
Thermal rating (°C)	85
Can external diameter (mm)	76.9
Can total height (mm)	105.7
Can side thickness (mm)	1.00
Can base thickness (mm)	3.25

To obtain the dimensions of the winding and to characterize it accurately, two methods were followed.

Initially, it was analyzed using a non-destructive method. X-ray images of the capacitor were obtained using a CT scan. The CT scanner's precision is 50 µm, which is insufficient to measure the foils' thickness, especially the cathode foil. However, it is more than enough to obtain other relevant data. The images obtained, Fig. 5, Fig. 6, and Fig. 7 are helpful to measure the following data.

- The thickness of the can on the sides and base.
- The total dimensions of the winding, including the internal diameter ($D_{W\text{-}int}$), the external diameter ($D_{W\text{-}ext}$), and the height (L_W). It also helped to measure the length of the extended

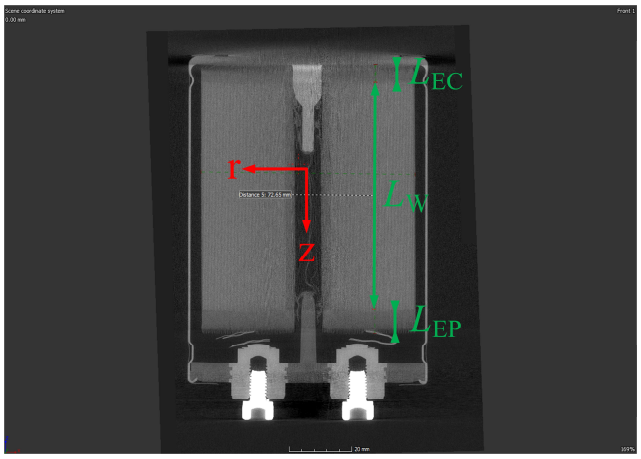

Fig. 5: Vertical cross-section of the capacitor.

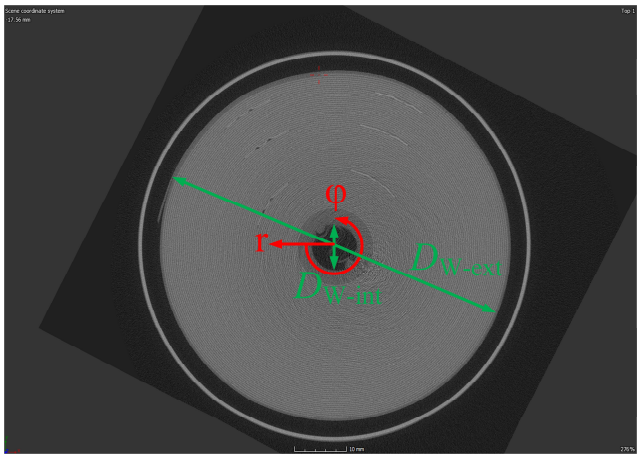

Fig. 6: Horizontal cross-section of the capacitor

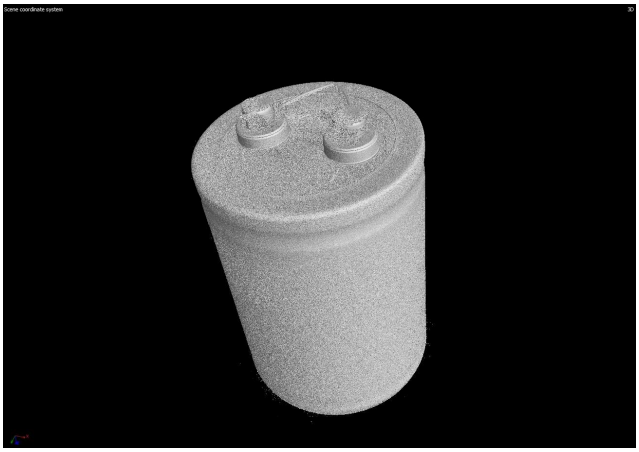

Fig. 7: 3D image obtained from the CT scan of the capacitor.

cathode (L_{EC}) and the length of the extended paper (L_{EP}) with the capacitor assembled

- The pitch of the winding. The pitch is the increase in the winding radius for every turn; this includes the anode, the cathode, and the papers soaked in electrolyte. This data was obtained by counting the number of turns in a 10 mm section of one winding radius.

Fig. 5 is helpful to do a preliminary analysis of the dissipation through the capacitor terminals. It can be seen clearly, that the screw terminals are connected to the winding with two aluminum foils with a small cross-section and are relatively long. These foils are marked as tabs in Fig. 4. Despite being made of aluminum, the small cross-section and its length might create a high thermal resistance through the terminals. The terminals' thermal resistance will be discussed when the winding thermal characteristics are discussed.

Afterward, the capacitor was cut and torn apart to measure the winding's foils' thickness and validate some of the CT scan measurements. Fig. 8 shows the capacitor cut in half. The capacitor was cut at a known angle of 30 degrees to make it easier to count the number of layers per mm with a digital microscope's help if necessary. As shown in Fig. 8, the tape that holds the capacitor rolled was not cut, keeping the winding compressed and avoiding any changes in its dimensions.

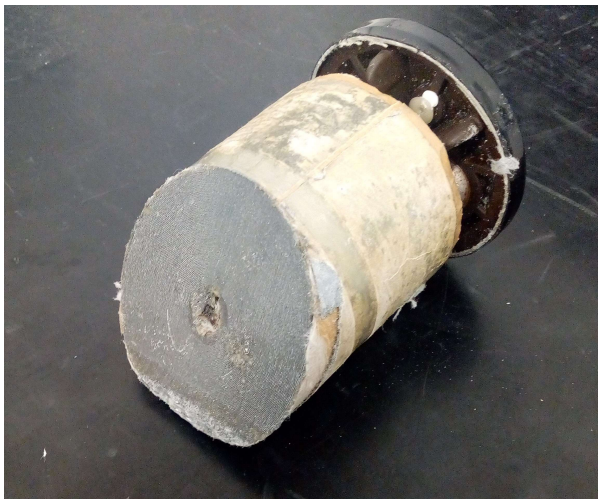

Fig. 8: Capacitor cut in half for measuring purposes.

The inferior half was used to measure the thickness of the different layers. The paper's thickness was not measured because it can vary when the different layers are torn apart. The paper is soaked in electrolyte and it may be slightly compressed when it is rolled. The thickness of the aluminum foils was measured, stacking several layers to avoid possible measuring errors. The length and section of the tabs connected to the terminals were measured as well.

The measured parameters are summarized in Table II. The number of layers per millimeter is one over the pitch.

TABLE II: WINDING DIMENSIONS

Parameter	Value
Winding external diameter [$D_{W\text{-}ext}$] (mm)	68.15
Winding internal diameter [$D_{W\text{-}int}$] (mm)	8.75
Winding total length [L_W] (mm)	72.65
Extended cathode length [L_{EC}] (mm)	5.80
Extended paper length [L_{EP}] (mm)	6.55
Anode foil thickness (µm)	120.00
Cathode foil thickness (µm)	35.00
Winding pitch (µm)	370.77
Number of layers per millimeter	2.70
Tabs section (mm^2)	1.20
Tabs length (mm)	22.00

The dimensions measured in the CT scan were similar to the dimensions measured directly in the capacitor. With a CT scan with higher precision, it could be possible to obtain all the capacitor's relevant data.

B. *Anisotropic characteristics analysis*

As mentioned before, the winding of the capacitor is modeled as an anisotropic material. To calculate the properties of this material, the weighted average is used. The weighted average is calculated considering the percentage of each material in the volume of the winding. The paper represents 58.20 % of the total volume in the case under study. The rest can be considered aluminum or aluminum oxide. The anode foil has a superficial layer of aluminum oxide, but the thickness is small. The relative permittivity (ε_r) of the aluminum oxide varies between 8 and 10, depending on its purity [4]. The anode surface is highly etched. The etching is done to increase the surface of the foil (A) and, in consequence, increase the capacitance (C) (3). In standard capacitors, the etching process increases the surface 3 to 120 times, according to [26], or 10 to 60 times for high voltage capacitors, according to [27]. With the winding dimensions, and the vacuum permittivity (ε_0), the thickness of the dielectric layer (d) can be calculated (3) to be around 5.3 µm in the worst scenario, distributed between the two faces of the anode foil. It represents 4.4% of the volume of the foil.

$$C = \varepsilon_r \cdot \varepsilon_0 \cdot \frac{A}{d} \tag{3}$$

According to [3], the dielectric layer is as dense and thin as 1.1–1.5 $nm \cdot V^{-1}$. The capacitor under study is rated for 500 V, which means the dielectric thickness will probably be lower than the 5.3 µm calculated before. For this study, the thickness of 5.3 µm will be considered since it is a safer approach from a thermal perspective. The thermal conductivity of aluminum oxide is worse than the thermal conductivity of aluminum. Therefore, an anode foil with a thicker layer of aluminum oxide will have a higher thermal resistance.

The thermal properties, thermal conductivity (k), and specific heat (c_p) of the aluminum and aluminum oxide (abbreviated as Al and AlO) can be considered common knowledge, as well as density (ρ). Since the electrolyte properties are unknown without determining the exact electrolyte used, the values measured in [8] for the paper soaked in electrolyte (abbreviated as PE) are used.

Equations (4) and (5) are used to calculate the different thermal conductivities. In (4), the r axis (k_r) thermal conductivity is calculated considering the different layers' thermal resistance to be in series. In (5), the thermal conductivities in the φ and z axis (k_φ and k_z) are calculated considering the different layers' thermal resistance to be in parallel. The percentage of the total volume of each material is represented by α_{Al}, α_{AlO}, and α_{PE}.

$$k_r = \frac{k_{Al} \cdot k_{AlO} \cdot k_{PE}}{k_{AlO} \cdot k_{PE} \cdot \alpha_{Al} + k_{Al} \cdot k_{PE} \cdot \alpha_{AlO} + k_{Al} \cdot k_{AlO} \cdot \alpha_{PE}} \quad (4)$$

$$k_z = k_\varphi = k_{Al} \cdot \alpha_{Al} + \alpha_{AlO} \cdot k_{AlO} + \alpha_{PE} \cdot k_{PE} \quad (5)$$

The density and the winding's specific heat capacity (abbreviated as W) are also calculated as the weighted average value. All the parameters can be found in Table III.

TABLE III: THERMAL PARAMETERS OF THE WINDING SIMPLIFICATION

Parameter	Value
α_{Al} (p.u.)	0.4037
α_{AlO} (p.u.)	0.0143
α_{PE} (p.u.)	0.5820
k_{Al} (W·m^{-1}·K^{-1})	240.00
k_{AlO} (W·m^{-1}·K^{-1})	30.00
k_{PE} (W·m^{-1}·K^{-1})	0.185
$k_{W\text{-}r}$ (W·m^{-1}·K^{-1})	0.318
$k_{W\text{-}z} = k_{W\text{-}\varphi}$ (W·m^{-1}·K^{-1})	97.425
$c_{p\text{-}Al}$ (J·kg^{-1}·K^{-1})	910.00
$c_{p\text{-}AlO}$ (J·kg^{-1}·K^{-1})	870.00
$c_{p\text{-}PE}$ (J·kg^{-1}·K^{-1})	640.00
$c_{p\text{-}W}$ (J·kg^{-1}·K^{-1})	752.29
ρ_{Al} (kg·m^{-3})	2700.00
ρ_{AlO} (kg·m^{-3})	3400.00
ρ_{PE} (kg·m^{-3})	1110.00
ρ_W (kg·m^{-3})	1784.63

The percentage of aluminum oxide might seem irrelevant. If not considered, the thermal conductivity in the φ and z axis variates 3%, k_φ and k_z without considering the Al_2O_3 layer are 100.43 W·m^{-1}·K^{-1}. If the Al_2O_3 layer is considered, this value decreases to 97.43 W·m^{-1}·K^{-1}. In the r axis, the conductivity is mainly determined by the paper soaked in electrolyte. Therefore, if the Al_2O_3 layer is not considered, the results are similar, with less than 1 % variation. The impact of considering the Al_2O_3 layer in the specific heat is negligible as well. Therefore, this layer can be eliminated from the analysis without substantially modifying the model's performance, increasing its simplicity for future studies.

C. *FEM simplified approach*

With the winding's anisotropic properties clear, it can be assessed whether the terminals will impact the thermal response. The thermal resistance (R) of a heat conductor can be expressed as

$$R = \frac{A}{k \cdot L}, \quad (6)$$

being A the cross-sectional area, k the thermal conductivity, and L the length.

With the values presented in Table II and Table III, each tab's thermal resistance is 7.64 K·W^{-1}. The winding's thermal resistance in the vertical axis is 0.21 K·W^{-1}, more than 30 times smaller than the tabs thermal resistance. Therefore, it can be concluded that the terminals' power dissipation will be negligible for the capacitor analyzed. Despite its high thermal resistance, the terminals will not be

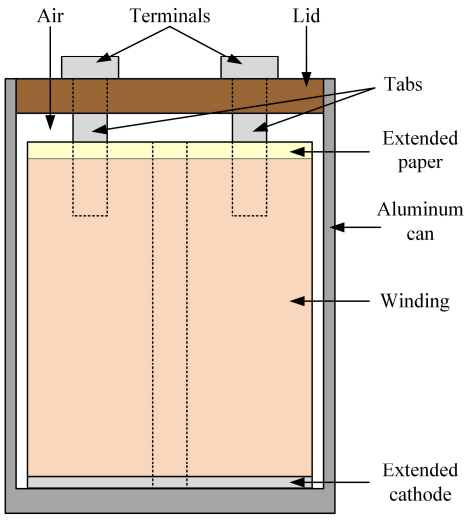

Fig. 9: Capacitor assembly including the extended cathode.

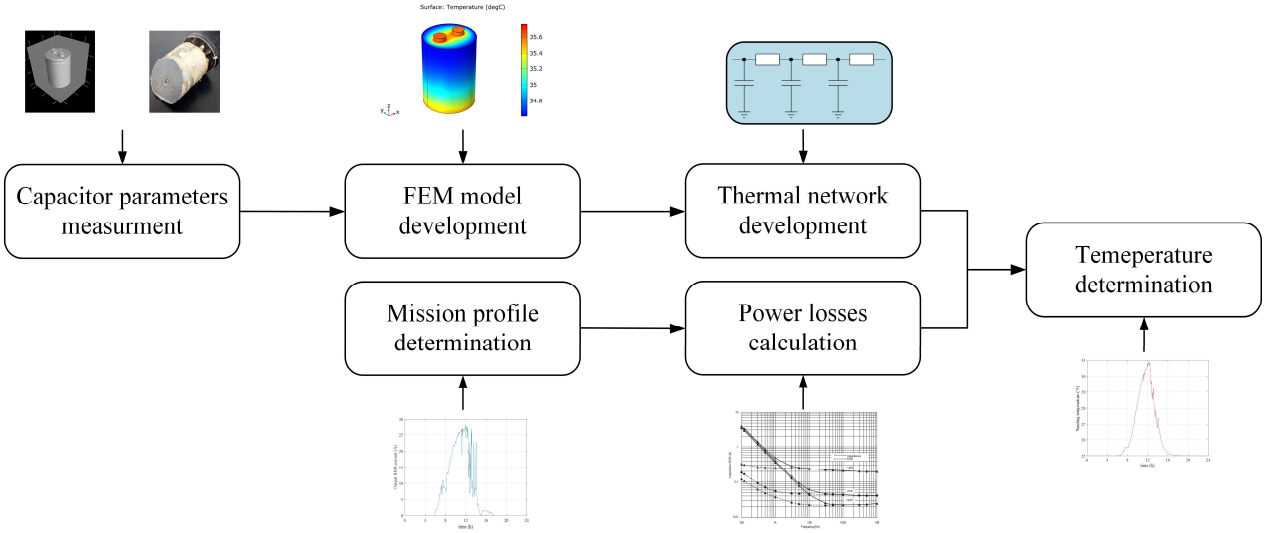

Fig. 10: Proposed approach for the FEM modeling.

removed from the model. It might be useful for future analyses.

The extended cathode (abbreviated as EC) in contact with the base of the can that encloses the capacitor is also modeled as an anisotropic material. In the vertical axis (z) and the angular coordinate (φ), the equivalent thermal conductivity is determined by the percentage of the cathode foil's volume. For a cathode foil with a thickness of 35 µm and a pitch of 422 µm, the total volume occupied by the cathode in the extended cathode region is only 8.29%. In the radial axis (r), the thermal conductivity is determined mainly by the air surrounding the cathode foil. The air's thermal conductivity is extremely low, below 0.05 $W \cdot m^{-1} \cdot K^{-1}$ at the expected temperatures.

Consequently, in the radial axis, the extended cathode can be considered adiabatic. Values can be found in Table IV. The specific heat and the equivalent material's density to the extended cathode will be calculated as the weighted value as done previously.

TABLE IV: THERMAL PARAMETERS OF THE EXTENDED CATHODE SIMPLIFICATION

Parameter	Value
k_{Air} ($W \cdot m^{-1} \cdot K^{-1}$)	<0.05
$k_{EC\text{-}r}$ ($W \cdot m^{-1} \cdot K^{-1}$)	<0.05
$k_{EC\text{-}z} = k_{EC\text{-}\varphi}$ ($W \cdot m^{-1} \cdot K^{-1}$)	19.89
$c_{p\text{-}Air}$ ($J \cdot kg^{-1} \cdot K^{-1}$)	1.01
$c_{p\text{-}EC}$ ($J \cdot kg^{-1} \cdot K^{-1}$)	75.53
ρ_{Air} ($kg \cdot m^{-3}$)	1.23
ρ_{EC} ($kg \cdot m^{-3}$)	224.10

The lid applies pressure to the winding using three ribbons with a small section directly pressing the extended paper. In Fig. 4, this lid and its ribbons are marked with the label Phenolic/Nylon cover with Centering Peg. The power flux through the extended paper, the ribbons, and the lid to the ambient can be considered zero. Consequently, the lid is modeled as a cylindrical piece. Between the extended paper and the lid an air gap is considered. The ribbons mentioned above have been omitted from the model.

The last simplification to be implemented in the model is the distribution of the losses inside the capacitor. Since the winding is modeled as a unique solid, the losses will be distributed uniformly inside the capacitor.

With all the data presented, it is possible to develop the capacitor's model following the basic structure presented in Fig. 9 and follow the approach proposed in Fig. 10.

IV. SIMPLIFICATIONS VALIDATION.

To ensure that the simplifications do not lead to erroneous results, it is necessary to compare the results considering an anisotropic model with a model considering the real internal structure. As it has been stated, it is unachievable to model the whole winding. To overcome this limitation, the results are compared for just a portion of the total winding. Only seven turns are considered, and a height of the capacitor of 20 mm. The equivalent model using an anisotropic material is implemented, and the results are compared. Only part of the winding is simulated, not including the can and neither the capacitor terminals. The goal is to keep the model simple to maintain the number of finite elements low. The simulated winding portion base is placed in the XY plane, i.e., the same orientation showed in Fig. 9.

The 3D models have been developed with CAD software, Solidworks, and the FEM analysis using COMSOL. All the FEM simulations performed for this paper use the same software.

The power losses for the model, including the internal foils, will be distributed half in the anode foil and half in the electrolyte solution. This assumption is reasonable [5]. The effect of the temperature in the electrolyte's electric resistance [28] is not considered because it will increment the model's complexity. It can be considered after obtaining a thermal network of the capacitor.

For the FEM simulations, the total power generated in the winding (P_W) is fixed to 10 W. The temperature (T_{ref}) on the extended cathode base and the winded capacitor's outer sides is set to 20 °C.

P_W and T_{ref} were selected to obtain graphic results easy to understand and easy to operate. The chosen values do not represent any specific case and are just chosen to get comparable results.

The simulation results show that the simplifications applied are acceptable since they are very close, less than 3% of error. Fig. 11 shows the results for the model considering the real structure. It is possible to see that the power dissipation is mainly on the vertical axis. It is possible to observe the structure in the temperature distribution but only in the base. In the superior part of the

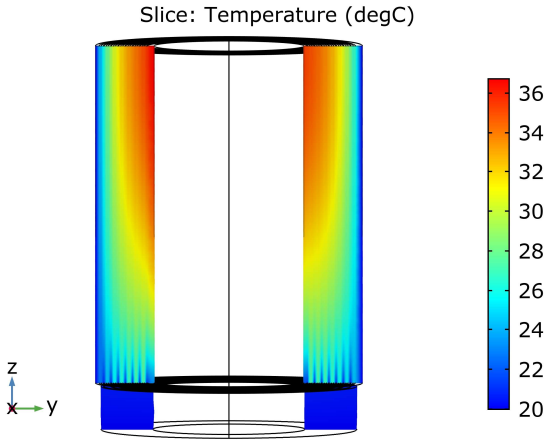

Fig. 11: Temperature distribution inside the capacitor considering the real structure.

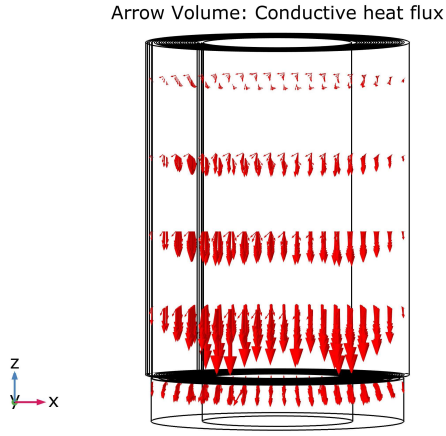

Fig. 12: Power flux inside the capacitor winding considering the real structure.

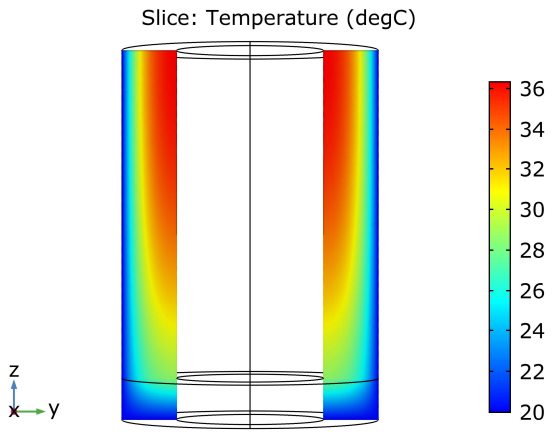

Fig. 13: Temperature distribution inside the capacitor considering an anistropic material.

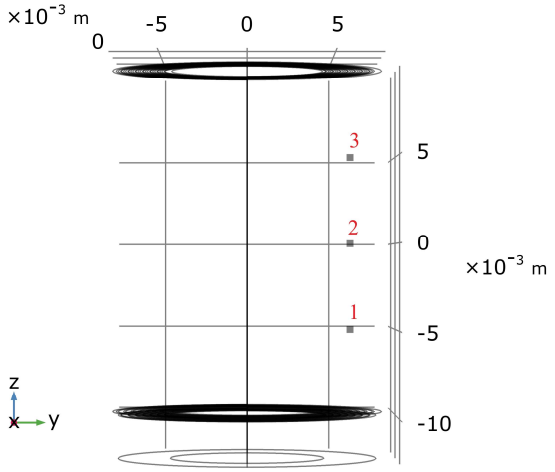

Fig. 14: Location of the temperature measurement points 1 to 3.

simulated winding, the temperature distribution is homogeneous.

Fig. 12 shows the power flux in the capacitor. This confirms the hypothesis that most of the power is dissipated through the extended cathode and the capacitor's base.

The vertical thermal conduction will be more exaggerated when considering the whole winding since its sides are surrounded by air that is a poor heat conductor.

The results considering the anisotropic material are similar, as shown in Fig. 13. The power flux, as expected, is dominant in the vertical axis due to the anisotropic properties of the material implemented in the simulation.

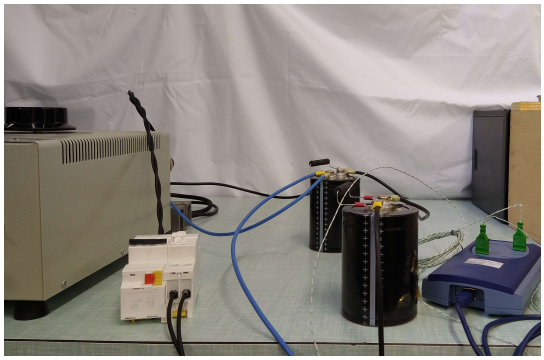

Fig. 15: Setup for the capacitor experimental tests.

The temperature increase has been measured at three winding points to compare the two models' results. Fig. 14 shows the position of the three points in the winding. The *x* and *y* coordinate are the same for the three capacitors, 0 mm and 6 mm. The *z* coordinate is -5 mm, 0 mm, and 5 mm, respectively, for the three points. The measured values and the error are summarized in Table V. The error between the different points is inferior to 4 %. Therefore, confirming the similarity between the two models.

TABLE V: COMPARISON OF THE RESULTS OBTAINED WITH THE REAL STRUCTURE AND THE ANISOTROPIC SIMPLIFICATION

Point	ΔT real structure (K)	ΔT anisotropic (K)	Error (%)
1	8.66	8.82	1.85
2	11.00	10.98	-0.25
3	12.40	12.00	-3.22

The maximum temperature increase (ΔT_W) measured in the simulation with the real structure is 17.02 °C. For the model considering the anisotropic material, the maximum temperature increase is 16.36 °C.

The thermal resistance (R_W) from the hottest point of the winding to the fixed temperature in the base or on the sides (T_{ref}) is 1.702 K·W^{-1} for the model considering the real structure and 1.636 K·W^{-1} for the model considering the simplifications. These values were calculated in steady-state (7), considering the power generated at the winding (P_W) and the reference temperature (T_{ref}).

$$R_W = \frac{\Delta T_W}{P_W} = \frac{T_W - T_{ref}}{P_W} \quad (7)$$

The error of the model considering the simplifications is inferior to 4%. It can be concluded that the simplifications applied to the model are acceptable.

The applied simplifications help to reduce substantially the number of elements used in the simulation. The model considering the internal geometry has slightly more than 3.25 million elements. The model considering an anisotropic material for the winding has only 23 thousand elements – more than a hundred times smaller.

Trying to simulate the whole capacitor, including the internal geometry, is hardly achievable. The entire capacitor's volume is more than a hundred times bigger than the one that has been simulated. This will lead to a FEM model with an enormous number of elements.

V. MODEL DEVELOPMENT AND RESULTS COMPARISON

The methodology proposed is used to create a model for the capacitor B43564A6278M000 from EPCOS [25]. A capacitor with this exact reference has been tested under controlled circumstances. The results obtained from the real measurements are compared with the results obtained from simulations.

A. *Capacitor experimental tests*

The tested capacitor was mounted on a wooden table; therefore, the base's heat dissipation can be considered zero. The terminals are connected to two wires connecting the capacitor with the equipment used to test the capacitor, see Fig. 15. The cables have a small copper section and are covered with plastic with good insulation properties. Together with the tabs high thermal resistance, the heat dissipation through the terminals can be considered zero as well. Therefore, there is only dissipation through the sides of the can.

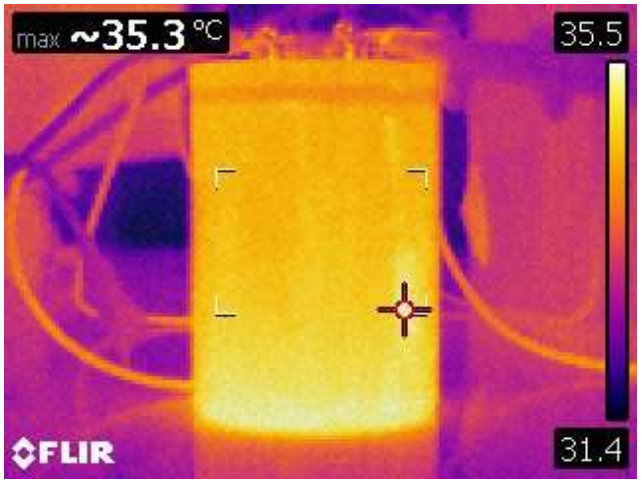

Fig. 16: Steady-state temperature distribution on the can surface for the capacitor operating under the fixed conditions.

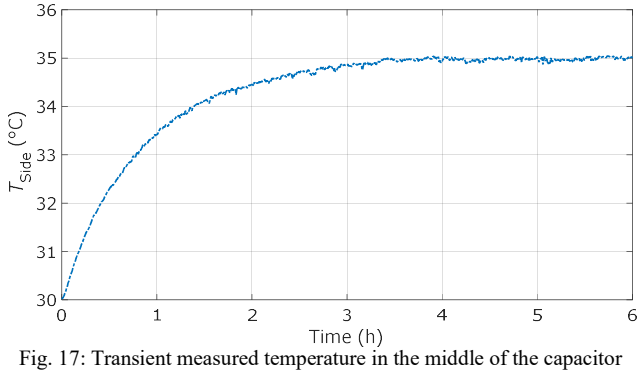

Fig. 17: Transient measured temperature in the middle of the capacitor side, T_{Side}.

The capacitor was tested using a ripple current capacitor tester [29], the average voltage was fixed to 400 V, and the current ripple was fixed to 6.5 A_{RMS}, at a fixed frequency of 100 Hz. The ambient temperature during the tests was 30 °C. Unfortunately, the capacitor was not fitted with a thermocouple. The addition of a thermocouple is a feature that must be added during the capacitor's manufacturing stage.

The capacitor was tested until it reached a stationary state. Fig. 16 shows the steady-state temperature distribution in the can under the described conditions. It is possible to see that the temperature is uniformly distributed in the capacitor. However, the base shows a slightly higher temperature. It is normal considering that the power flows from the winding to the base of the can and then is dissipated in the sides of the can. The maximum temperature measured in the can's base is 35.5 °C, and the temperature in the middle of the can might be assumed to be 35 °C. Fig. 17 shows the measured temperature in the middle of the can during the test. The steady-state temperature is reached after four hours of operation approximately. The temperature was measured with a K-type thermocouple and a datalogger. The measured steady-state temperature with the thermal camera, Fig. 16, is consistent with the final temperature measured with the K-type thermocouple, Fig. 17. Unfortunately, the capacitor did not have a thermal measurement inside the winding. Therefore, the internal temperature is not available.

The temperature increase is low because the total losses are low.

It is necessary to determine the capacitor's equivalent series resistance, *ESR*, to determine the power losses during the performed test. The *ESR* value is not constant with frequency due to the electrolyte properties and its interface with the dielectric layer [5]. The measured *ESR* at the tested frequency, 100 Hz, was 27.8 mΩ. With the injected current, the average capacitor losses (P_{Cap}) are 1.175 W.

B. *Ambient heat dissipation determination*

For the FEM simulation with the model considering the anisotropic material, the can's sides' heat dissipation is modeled with a heat convection coefficient to reduce the simulation time. This convection coefficient is obtained from a thermal simulation, including the natural convection and the capacitor's radiation, and considering the capacitor a solid element. Consequently, allowing the usage of a 2D axisymmetric simulation and making it faster to simulate.

In this first simulation, the capacitor is modeled as a solid element sitting on an isolated surface and surrounded by air. The air regime shall be simulated as laminar because the Raleigh number (8) associated with the system is below 10^9 [30].

$$\mathrm{Ra} = \frac{g \cdot \alpha_p \cdot \Delta T \cdot h^3}{\kappa \cdot \nu} \tag{8}$$

The parameters in equation (8) can be found in Table VI.

TABLE VI: PARAMETERS FOR CALCULATING THE RALEIGH NUMBER

Parameter	Value
Gravity [g] ($m \cdot s^{-2}$)	9.81
Coefficient of thermal expansion of air [α_p] (K^{-1})	$3.32 \cdot 10^{-3}$
Expected temperature increase [ΔT] (K)	5.0
Height of the cap [h] (m)	$105.7 \cdot 10^{-3}$
Thermal diffusivity of air [κ] ($m^2 \cdot s^{-1}$)	$23.07 \cdot 10^{-6}$
Kinematic viscosity of air [ν] ($m^2 \cdot s^{-1}$)	$15.98 \cdot 10^{-6}$

The emissivity of the can, including the isolating PVC sleeve, can be assumed to be 0.85 [8], [31].

With these values, the results can be seen in Fig. 18. The can's surface temperature is 35 °C. Due to the capacitor's solid geometry, it is uniform in all the capacitor's lateral. The results match the temperature seen in the real measurements.

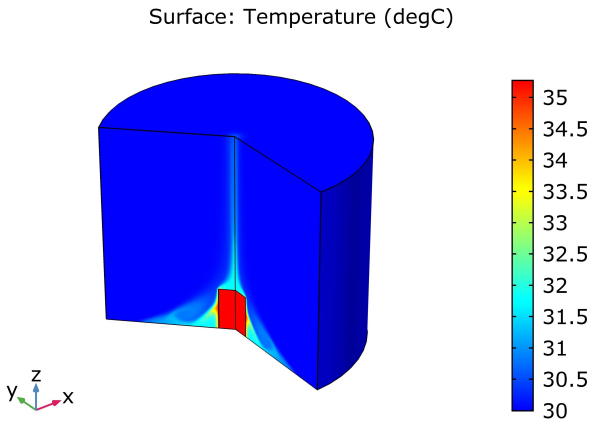

Fig. 18: Capacitor surface temperature considering it as a solid with natural convection and radiation.

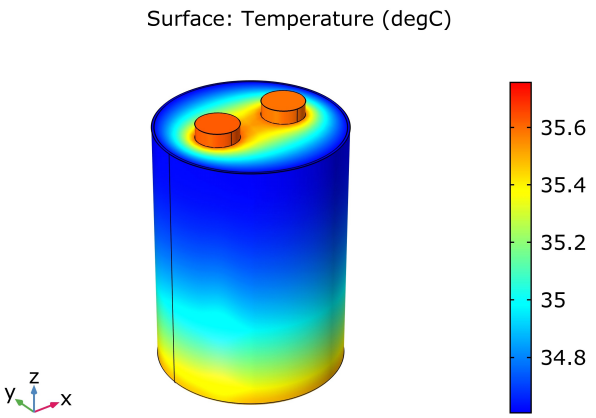

Fig. 19: Temperature distribution at the can of the capacitor considering the winding as an anistropic material.

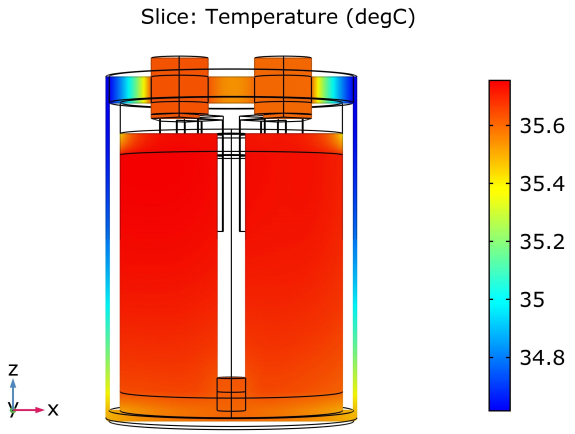

Fig. 20: Temperature distribution of the interior of the capacitor considering the winding as an anistropic material.

From this simulation, the convection coefficient (h) to apply in the FEM simulation of the anisotropic model is obtained using (9) and (10).

$$\Delta T_{\mathrm{c-a}} = R_{\mathrm{c-a}} \cdot P_{\mathrm{Cap}} \tag{9}$$

$$R_{\mathrm{c-a}} = \frac{1}{h \cdot A_{\mathrm{c}}} \tag{10}$$

Being A_{c}, the surface of the side of the can that encloses the capacitor, and $R_{\mathrm{c\text{-}a}}$, the thermal resistance from the, can to the ambient.

C. *Capacitor thermal model development*

The thermal coefficient used in the simulation implementing the anisotropic model is h = 9.49 $\mathrm{W \cdot m^{-1} \cdot K^{-1}}$. This is a simplification since the radiation is strongly dependent on the temperature. However, it is realistic since the temperature variation will be low.

Fig. 19 shows the result of the simulation for the described conditions. As it is possible to see, the outside temperature is consistent with the real measurements' results, Fig. 16. The can's base temperature is higher than in the superior half, confirming that the power flux goes from the winding to the base and dissipates through the can's lateral. The maximum temperature measured in the can is 35.45 °C, extremely close to the maximum value measured with the thermal camera.

In Fig. 20, the temperature inside the winding is shown. The hottest temperature in the winding is 35.76 °C. The difference with the can is low, but it is reasonable. The test performed with the capacitor dissipates a low amount of power; therefore, the temperature increase is low. In Fig. 20, the capacitor interior air domain surrounding the winding has been removed to increase the results' understandability.

It is worth stating that the model only required 700 thousand elements, which is a considerably low value. With this number of elements, a FEM simulation can be run without needing expensive simulation equipment.

The capacitor manufacturer provided a thermal network for the steady-state analysis of this capacitor with natural convection, Fig. 21. This thermal network is not available online and shall be requested from the manufacturer. The authors had no problem having access to this information after asking it. Considering that the dissipation in the terminals is zero, i.e., considering R24 as infinite, and the dissipation in the base is zero, i.e., considering R34a as infinite, the expected temperature in the core of the capacitor is 35.05 °C, similar to the values obtained.

Since the results obtained with the proposed method seem consistent, it is interesting to get more information. The next step is to extract a simple thermal network of the capacitor, including the thermal capacitance.

The thermal network can be implemented, as shown in Fig. 22 and Fig. 23. For both figures, T_{Winding} refers to the hottest temperature in the winding. T_{Base} refers to the average temperature on the base. T_{Side} refers to the average temperature on the side. Finally, T_{Amb} refers to ambient temperature.

The thermal resistances of the proposed thermal network have been calculated with the steady-state temperatures measured in the anisotropic model simulation, Fig. 19 and Fig. 20. It has been assumed that all the power dissipated in the capacitor (P_{Cap}) flows from the winding to the can's base, next to the can's sides, and finally to the ambient. The thermal resistance ($R_{\mathrm{i\text{-}j}}$) between two points, i and j, is calculated as

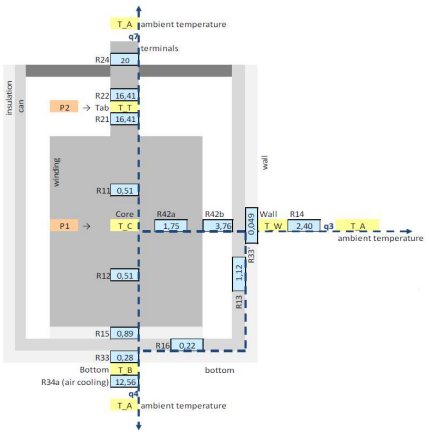

Fig. 21: Thermal network of the capacitor under natural convection. Source: EPCOS.

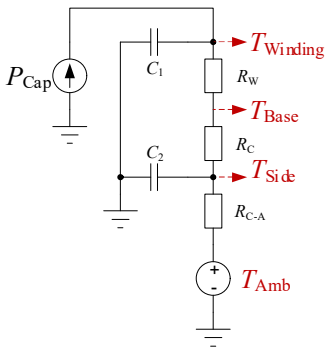

Fig. 22: Proposed thermal network for the model under study.

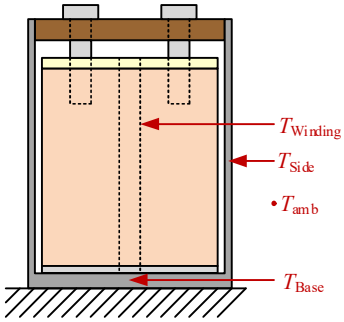

Fig. 23: Temperature measurement points of the thermal network proposed.

$$R_{i-j} = \frac{\Delta T_{i-j}}{P_{Cap}} = \frac{T_i - T_j}{P_{Cap}}. \quad (11)$$

However, the thermal capacitances (C_1 and C_2) must be obtained from the transient thermal response. A transient thermal analysis is performed with the FE model presented previously in this section. As has been explained previously, the capacitor lacks a temperature measurement inside the winding. Therefore, it is not possible to compare the winding temperature simulation results with the experimental setup.

For the steady-state analysis, the power dissipated in the capacitor was modeled as a constant value, P_{Cap}. However, for the transient thermal analysis, the power should no longer be considered constant to characterize the thermal network properly.

The power dissipated in the capacitor can be expressed as

$$P(t) = ESR_{100Hz} \cdot I(t)^2 = ESR_{100Hz} \cdot 2 \cdot {I_{RMS}}^2 \cdot \cos(\omega t)^2, \quad (12)$$

being $ESR_{100Hz} \cdot {I_{RMS}}^2$ the same as P_{Cap}.

Consequently, (12) can be re-written as

$$P(t) = P_{Cap} + P_{Cap} \cdot \cos(2\omega t). \quad (13)$$

Equation (13) has a constant term and a term pulsating twice the current frequency, i.e., 200 Hz.

A transient simulation with the FEM model was done, defining (13) as the capacitor power losses. The first graph of Fig. 24 shows a comparison of the measured side temperature increase of the capacitor,

$$\Delta T_{Side} = T_{Side} - T_{Amb}, \quad (14)$$

and the simulated side temperature increase with the FEM model. The second graph of Fig. 24 shows the per-unit error between the simulation results and the experimental results, expressed as

$$\text{error} = \frac{\Delta T_{Side-sim} - \Delta T_{Side}}{\Delta T_{Side}}. \quad (15)$$

The error is not calculated in the first 8 minutes of operation for the sake of clarity in the graph. ΔT_{Side} tends to zero, and consequently, the error tends to infinite.

During the transient, the error is always below 0.08 pu and is lower than 0.05 pu during most of it. The steady-state error is smaller than 0.025 pu in absolute value. Therefore, the error between the simulation and the experimental results is small enough to consider the simulation model correct.

Fig. 25 shows the simulated capacitor's hottest point temperature over time.

The capacitor's hottest point temperature shows the typical response to a step of power. This behavior is caused by the constant term of (13). Additionally, it can be observed that the temperature oscillation at 200 Hz is inappreciable in the graph. The oscillation is below 0.01 °C. Therefore, it can be concluded that the pulsating term of (13) can be neglected for future analyses.

The C_1 and C_2 values have been calculated by matching the proposed thermal network transient response to the response shown in Fig. 24 and Fig. 25. The curve fitting tool from MATLAB was used to perform this operation.

The parameters of the proposed thermal network can be found in Table VII.

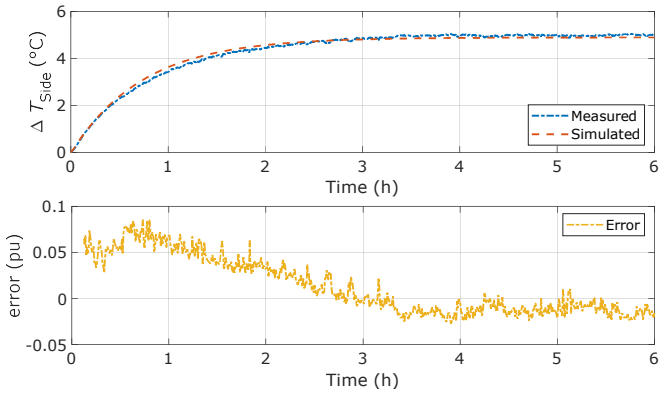

Fig. 24: Side temperature increase comparison between the experimental results and the simulation results. Error between the simulation results and the experimental results

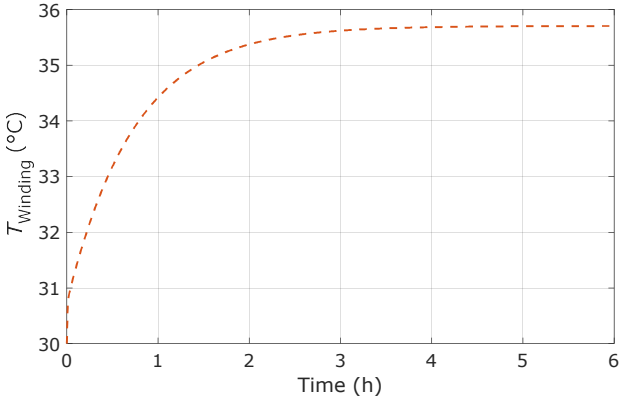

Fig. 25: Hottest point temperature evolution considering the winding as an anisotropic material.

TABLE VII: PARAMETERS FOR THE PROPOSED THERMAL NETWORK

Parameter	Value
Winding thermal resistance [R_W] (K·W^{-1})	0.1540
Can thermal resistance [R_C] (K·W^{-1})	0.5362
Can to ambient thermal resistance [$R_{C\text{-}A}$] (K·W^{-1})	4.1617
Capacitor thermal capacitance 1 [C_1] (J·K^{-1})	28.84
Capacitor thermal capacitance 2 [C_2] (J·K^{-1})	610.06

VI. CASE STUDY

A mission profile analysis is performed to validate the application of the proposed model. The proposed model is compared with the model provided by the manufacturer to compare the obtained results.

For the validation is assumed that the capacitor is used in the DC-link of a single-phase PV inverter. With the PV inverter's output current, the capacitor's current can be calculated easily [32].

The analysis is done with a one-day profile obtained from measurements of a PV inverter operating in the field. Fig. 26 shows the RMS output current for 24 hours of operation, with a sampling time of 15 seconds.

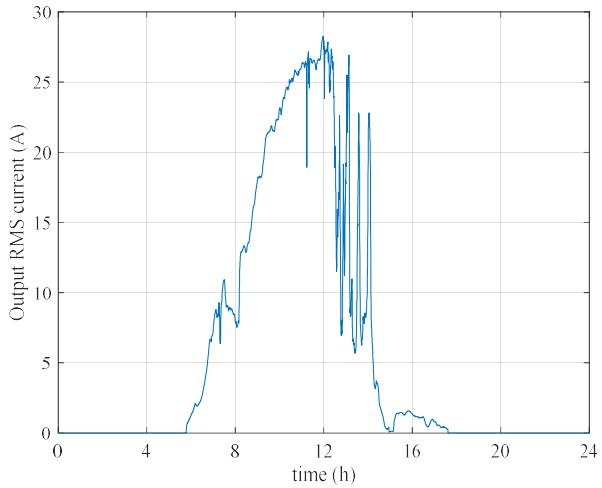

Fig. 26: PV generation profile used to implement the mission profile analysis.

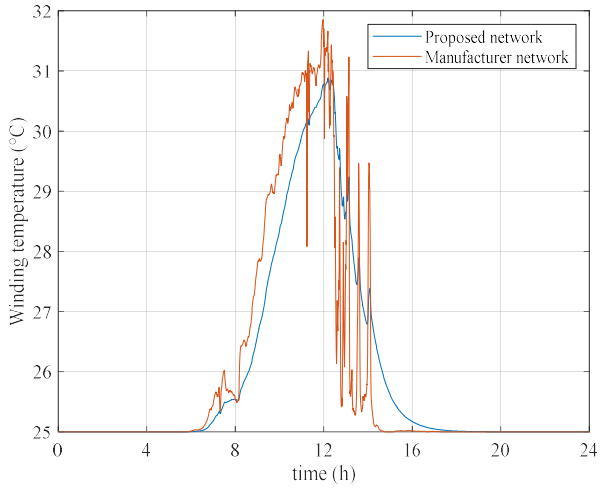

Fig. 27: Winding maximum temperature comparison considering the proposed method and the thermal network provided by the manufacturer.

The proposed thermal network, Fig. 22 and Fig. 23, is compared with the thermal network provided by the manufacturer, Fig. 21. The maximum winding temperature for both thermal networks is shown in Fig. 27.

The results differ substantially. The shape of the temperature during the operation of the converter is different. The results obtained with the manufacturer's thermal network show a series of fast transients that are especially relevant between hours 12 and 16. These spikes have the same shape as the spikes seen in Fig. 26. The results obtained with the proposed thermal network show that these spikes are filtered. The maximum difference between both thermal networks is superior to three degrees at some points.

The difference in the results can be explained by the lack of thermal capacitance in the manufacturer's thermal network. The proposed thermal network includes two thermal capacitances. Therefore, these fast transients are filtered.

According to our FEM simulation results, the capacitor has a low-pass filter behavior, Fig. 25. Therefore, it can be assumed that the capacitor's thermal network should have some capacitive elements to replicate the low-pass behavior properly. Consequently, the winding temperature calculated with the manufacturer's thermal network will probably lead to wrong temperature estimations during fast transients and distort the reliability analysis results.

VII. CONCLUSIONS

The model proposed was proved to replicate the behavior of the rolled layers of the capacitor accurately and, at the same time, substantially reduce the resource consumption for simulation. This allows introducing this model in a more complex system and evaluating the interaction with other elements.

The impact of the aluminum oxide layer was analyzed in the paper. Its impact on the thermal response is small, and therefore, it can be obviated for future analyses.

Instead of using a FEM model obtained from measurements with the capacitor in operation, the proposed method is based on dimensional measurements. This helps to reduce the time spent on the development of the model. The thermal properties of the materials used inside the capacitor are well studied, easing the model's implementation.

The model allows the extraction of a complex thermal network that can be used for the thermal characterization of capacitors. The proposed method is suitable for off-the-shelf capacitors.

ACKNOWLEDGMENT

The authors would like to thank the research group in battery systems (AG Batteriesysteme) from the University of Applied Sciences Würzburg-Schweinfurt (FHWS) and Preh GmbH for their help with the obtention of the CT scan images used in this paper.

BIBLIOGRAPHY

[1] H. Wang and F. Blaabjerg, "Reliability of Capacitors for DC-Link Applications in Power Electronic Converters—An Overview," *IEEE Transactions on industry applications,* vol. 50, no. 5, pp. 3569-3578, 2014.

[2] S. G. Parler Jr., "Deriving Lifetime Multipliers for Electrolytic Capacitors," *IEEE Power Electronics Society Newsletter,* vol. 16, no. 1, pp. 11-12, 2004.

[3] Nippon Chemi-Con, "Technical Note- Judicious Use of Aluminum Electrolytic Capacitors," Nippon Chemi-Con, Tokyo, 2013.

[4] Cornell Dubilier, "Aluminum Electrolytic Capacitor Application Guide," Cornell Dubilier, Liberty.

[5] H. Ma and L. Wang, "Fault Diagnosis and Failure Prediction of Aluminium Electrolytic Capacitors in Power Electronic Converters," in *IECON Proceedings (Industrial Electronics Conference)*, Raleigh, 2005.

[6] J. L. Stevens, J. S. Shaffer and J. T. Vandenham, "The service life of large aluminum electrolytic capacitors: Effects of construction and application," *IEEE Transactions on Industry Applications,* vol. 38, no. 5, pp. 1441-1446, 2002.

[7] R. S. Alwitt and R. G. Hills, "The Chemistry of Failure of Aluminum Electrolytic Capacitors," *IEEE Transactions on Parts, Materials and Packaging,* vol. 1, no. 2, pp. 28-34, 1965.

[8] S. G. Parler Jr., "Thermal Modeling of Aluminum Electrolytic Capacitors," in *Conference Record of the 1999 IEEE Industry Applications Conference. Thirty-Forth IAS Annual Meeting (Cat. No.99CH36370)*, Phoenix, 1999.

[9] S. G. Parler Jr. and L. Macomber, "Predicting Operating Temperature and Expected Lifetime of Aluminum-Electrolytic Bus Capacitors with Thermal Modeling," in *PCIM*, Nuremberg, 1999.

[10] J. L. Stevens, J. D. Sauer and J. S. Shaffer, "MODELING AND IMPROVING HEAT DISSIPATION FROM LARGE ALUMINUM ELECTROLYTIC CAPACITORS: II," in *IEEE Industry Applications Conference. Thirty-Second IAS Annual Meeting*, New Orleans, 1997.

[11] J. L. Stevens, J. D. Sauer and J. S. Shaffer, "FURTHER IMPROVING HEAT DISSIPATION FROM LARGE ALUMINUM ELECTROLYTIC CAPACITORS," in *IEEE Industry Applications Conference. Thirty-Third IAS Annual Meeting*, Saint Louis, 1998.

[12] H. Wang, Q. Wang and H. Wang, "A Lumped Thermal Model Including Thermal Coupling Effects and Boundary Conditions for Capacitor Banks," in *2018 International Power Electronics Conference (IPEC-Niigata 2018 - ECCE Asia)*, Niigata, 2018.

[13] T. Furukawa, D. Senzai and T. Yoshida, "Electrolytic Capacitor Thermal Model and Life Study for Forklift Motor Drive Application," in *2013 World Electric Vehicle Symposium and Exhibition (EVS27)*, Barcelona, 2013.

[14] S. Prasanth, M. H. Mohamed Sathik, F. Sasongko, T. C. Seng, P. Yaxin and R. Simanjorang, "Condition Monitoring of Electrolytic Capacitor based on ESR Estimation and Thermal Impedance model using Improved Power Loss Computation," in *2018 International Power Electronics Conference, IPEC-Niigata - ECCE Asia 2018*, Niigata, 2018.

[15] P. Freiburger, "Transient Thermal Modelling of Aluminum Electrolytic Capacitors Under Varying Mounting Boundary Conditions," in *THERMINIC 2015 - 21st International Workshop on Thermal Investigations of ICs and Systems*, Paris, 2015.

[16] M. H. El-Husseini, P. Venet, G. Rojat and C. Joubert, "Thermal Simulation for Geometric Optimization of Metallized Polypropylene Film Capacitors," *IEEE Transactions on Industry Applications,* vol. 38, no. 3, pp. 713-718, 2002.

[17] J. R. MacDonald, M. A. Schneider, M. C. Schalnat and J. B. Ennis, "Thermal Modeling of High Temperature Power Conversion," in *2012 IEEE International Power Modulator and High Voltage Conference (IPMHVC)*, San Diego, CA, USA, 2012.

[18] Z. Na, "A Study of Electrolytic Capacitor's Thermal Conductivity, Behavior and Measurement," in *THERMINIC 2016 - 22nd International Workshop on Thermal Investigations of ICs and Systems*, Budapest, 2016.

[19] J. Chen, W. Chen, J. Li, X. Zhang and P. Sun, "Lifetime Assessment of DC Link Electrolytic Capacitor of Wind Power Converter Based on Operational Condition," in *ICHVE 2016 - 2016 IEEE International Conference on High Voltage Engineering and Application*, Chengdu, 2016.

[20] C.-S. Yun, P. Malberti, M. Ciappa and W. Fichtner, "Thermal Component Model for Electrothermal Analysis of IGBT Module Systems," *IEEE Transactions on Advanced Packaging,* vol. 24, no. 3, pp. 401-406, 2001.

[21] A. S. Bahman, K. Ma, P. Ghimire, F. Iannuzzo and F. Blaabjerg, "A 3-D-Lumped Thermal Network Model for Long-Term Load Profiles Analysis in High-Power IGBT Modules," *IEEE Journal of Emerging and Selected Topics in Power Electronics,* vol. 4, no. 3, pp. 1050-1063, 2016.

[22] A. S. Bahman, K. Ma and F. Blaabjerg, "A Lumped Thermal Model Including Thermal Coupling and Thermal Boundary Conditions for High-Power IGBT Modules," *IEEE Transactions on Power Electronics,* vol. 33, no. 3, pp. 2518-2530, 2018.

[23] C. Tang and T. Thiringer, "Thermal modelling of a multichip IGPT power module," in *2019 21st European Conference on Power Electronics and Applications (EPE '19 ECCE Europe)*, Genova, Italy, 2019.

[24] T. A. Kent and J. S. Shaffer, "Heat Dissipation Aluminum Electrolytic Capacitor". US Patent 4546415, 8 October 1985.

[25] EPCOS AG, "Capacitors with Screw Terminals B43564/B43584," EPCOS AG, Munich, 2002.

[26] ELNA, "How Capacitors Work – Aluminum Electrolytic Capacitors Principles," 2013. [Online]. Available: http://www.elna.co.jp/en/capacitor/alumi/principle.html. [Accessed 06 October 2019].

[27] Rubycon, "Aluminum Electrolytic Capacitor Technical Notes – Manufacturing Process," 2013. [Online]. Available: http://www.rubycon.co.jp/en/products/alumi/technote2.html#2. [Accessed 6 October 2019].

[28] M. A. Vogelsberger, T. Wiesinger and H. Ertl, "Life-Cycle Monitoring and Voltage-Managing Unit for DC-Link Electrolytic Capacitors in PWM Converters," *IEEE Transactions on Power Electronics,* vol. 26, no. 2, pp. 493-503, 2011.

[29] CHROMA ATE INC., "Ripple Current Tester Model 11800/11801/11810," 2014.

[30] COMSOL, "Natural Convection Cooling of a Vacuum Flask," [Online]. Available: https://www.comsol.com/model/download/543521/models.heat.vacuum_flask.pdf. [Accessed 24 07 2019].

[31] M. L. Gasperi and N. Gollhardt, "Heat transfer model for capacitor banks," in *Conference Record of 1998 IEEE Industry Applications Conference. Thirty-Third IAS Annual Meeting*, Saint Louis, 1998.

[32] Y. Lei, C. Barth, S. Qin, W.-C. Liu, I. Moon, A. Stillwell, D. Chou, T. Foulkes, Z. Ye, Z. Liao and R. C. N. Pilawa-Podgurski, "A 2-kW Single-Phase Seven-Level Flying Capacitor Multilevel Inverter With an Active Energy Buffer," *IEEE Transactions on Power Electronics,* vol. 32, no. 11, pp. 8570-8581, 2017.

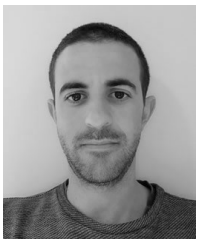

Tomàs Lledó-Ponsati was born in Barcelona, Spain, in 1990. He received his M.Sc. degree in Industrial Engineering from the Technical University of Catalunya (UPC) in 2013. After graduating, he worked for teknoCEA developing power converters. Since 2015 he is pursuing his Ph.D. studies. In 2018 he joined CITCEA-UPC to work on research projects related to power electronics. His main research interests are power converters based on wide-bandgap semiconductors and reliability analysis.

Amir Sajjad Bahman is currently an Associate Professor at the Center of Reliable Power Electronics (CORPE), Aalborg University, Denmark. His research interests include electro-thermo-mechanical modelling, packaging and reliability of power electronic systems and components. Dr. Bahman received the B.Sc. from Iran University of Science and Technology, in 2008, the M.Sc. from Chalmers University of Technology, Sweden in 2011 and the Ph.D. from Aalborg University, Denmark, in 2015 all in electrical engineering. He was a Visiting Scholar in the Department of Electrical Engineering, University of Arkansas, USA, in 2014. Moreover, he was with Danfoss Silicon Power, Germany in 2014 as the Thermal Design Engineer. Dr. Bahman is a senior member of the IEEE and currently serves as an Associate Editor for the IEEE the IEEE Transactions on Transportation Electrification, and Elsevier Microelectronics Reliability.

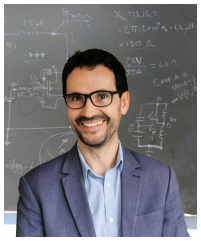

Francesco Iannuzzo (M'04-SM'12) is currently a professor at the Aalborg University, Denmark, where he is also part of CORPE (Center of Reliable Power Electronics). His research interests are in the field of reliability of power devices, including mission-profile-based life estimation, condition monitoring, failure modeling, and testing up to MW-scale modules under extreme conditions, like overvoltage, overcurrent, overtemperature, and short circuit. He is the author or co-author of +250 publications on journals and international conferences, three book chapters, and four patents. He has edited the recently-published Modern power electronic devices: physics, applications, and reliability book. Besides publication activity, over the past years, he has been invited for several technical seminars about reliability at first conferences as ISPSD, EPE, ECCE, PCIM, and APEC. Prof. Iannuzzo is the founder of the newborn Power Electronic Devices and Components journal with Elsevier and serves as Associate Editor for the IEEE Transactions on Industry Applications, the IEEE Journal of Emerging and Selected Topics in Power Electronics, and Elsevier Microelectronics Reliability. He is the vice-president of the IEEE IAS Power Electronic Devices and Components Committee. He was the general chair of ESREF 2018, the 29th European Symposium on Reliability of Electron Devices, Failure physics, and analysis, and has been appointed EPE-ECCE Europe General Chair in 2023.

Daniel Montesinos-Miracle was born in Barcelona, Spain, in 1975. He received the M.Sc. degree in Electrical Engineering from the School of Industrial Engineering of Barcelona (ETSEIB), Technical University of Catalonia (UPC), Barcelona, Spain, in 2000, and PhD degree from the Technical University of Catalonia (UPC), in 2008. In 2001 he joined Salicru Electronics, S.A., Santa Maria de Palautordera, Spain as a research and development engineer. Since 2001 he has been involved in the Centre of Technological Innovation in Static Converters and Drives (CITCEA-UPC) as a research collaborator. In 2005 he became a lecturer at Electrical Engineering Department, Polytechnic University of Catalonia (UPC). Since 2012 he is an Associate Professor at UPC. He has become the CITCEA-UPC director in 2016. In 2012, he co-founded teknoCEA, a spin-off company providing components, systems and services for power electronics research and manufacturing. His primary research interests are power electronics, drives and green energy converters.

Samuel Galceran-Arellano was born in Lleida, Spain, in 1971. He received the M.Sc. degree in electrical engineering and the Ph.D. degree from the Polytechnic University of Catalonia (UPC), Barcelona, Spain, in 1997 and 2002, respectively. In 1997, he joined the Electrical Engineering Department, UPC, as an Assistant Professor. He developed several projects for industry, and in 2001, he joined the Center of Technological Innovation in Static Converters and Drives (CITCEA-UPC), UPC, where he belongs to the CITCEA-UPC Directorate staff. His primary research interests are motor control and converters for power supplies and drives. He is Head of Electrical Engineering Department at UPC from 2014.